Ahmed M. Alotaibi
School of Mechanical Engineering,
Purdue University,
West Lafayette, IN 47907
e-mail: alotaib3@purdue.edu

Sohel Anwar[1]
Mem. ASME
Department of Mechanical Engineering,
IUPUI,
Indianapolis, IN 46202
e-mail: soanwar@iupui.edu

M. Terry Loghmani
School of Health and Rehabilitation Sciences,
IUPUI,
Indianapolis, IN 46202
e-mail: mloghman@iu.edu

Stanley Chien
Department of Electrical and
Computer Engineering,
IUPUI,
Indianapolis, IN 46202
e-mail: schien@iupui.edu

Force Sensing for an Instrument-Assisted Soft Tissue Manipulation Device

Instrument-assisted soft tissue manipulation (IASTM) is a form of mechanotherapy, e.g., massage, that uses rigid devices which may be machined or cast. The delivered force, which is a critical parameter during IASTM, is not measured and not standardized in current clinical IASTM practice. In addition to the force, the angle of treatment and stroke frequency play an important role during IASTM. For accurate IASTM treatment, there is a strong need to scientifically characterize the IASTM delivered force, angle of treatment, and stroke frequency. This paper presents a novel, mechatronic design of an IASTM device that can measure the localized pressure on the soft tissue in a clinical treatment. The proposed design uses a three-dimensional (3D) load cell, which can measure all three-dimensional force components simultaneously. The device design was implemented using an IMUduino microcontroller board which provides tool orientation angles. These orientation angles were used for coordinate transformation of the measured forces to the tool–skin interface. Additionally, the measured force value was used to compute the stroke frequency. This mechatronic IASTM tool was validated for force measurements in the direction of tool longitudinal axis using an electronic plate scale that provided the baseline force values to compare with the applied force values measured by the tool. The load cell measurements and the scale readings were found to agree within the expected degree of accuracy. [DOI: 10.1115/1.4036654]

Introduction

Mechanotherapies have been used for thousands of years to help people relieve their pain and musculoskeletal stresses by a variety of clinicians, including physical therapists, massage therapists, athletic trainers, chiropractors, and osteopathic physicians. Physical therapeutics includes different methods, all of which have been developed and modified to meet patients' satisfaction and well-being. IASTM is a type of mechanotherapy that provides a mechanical stimulus to the tissue. IASTM is a form of manual therapy; in essence, a massage technique that uses solid tools to improve the quality of injured or restricted tissue. The Graston Technique® (GT) is a modern day massage methodology based on IASTM using six different tools for different tasks and functions. These stainless steel instruments are illustrated in Fig. 1.

IASTM is often utilized in the treatment of soft tissue dysfunction. The method focuses on delivering controlled and precise forces to a targeted area of scar tissue or fibrosis. IASTM has been used widely for decades offering promising results for different conditions and tissues [1–8] and has been found to stimulate repair and reorganization of affected tissue [9]. However, the lack of force quantification has impeded the development of optimal dosing for best outcomes during IASTM procedures and has limited the understanding of its underlying biological mechanisms [10–12].

The GT was introduced to the world of physical rehabilitation by an athlete who suffered a debilitating knee injury during a water skiing accident. Left with resultant scar tissue from the injury that caused pain and restriction of motion and function in the affected tissues [13], he created various tools to treat the soft tissue surrounding his knee using his knowledge in machining. In 1994, TherapyCare Resources, Inc., the founding company of the Graston Technique®, was established in Indianapolis, IN [14]. GT has been recommended for use in the treatment of soft tissue injury (e.g., tendinopathies, trigger-points, hypertonicity, and myofascial pain).

In one study, GT treatment was found to improve shoulder motion in overhead athletes (softball, baseball, or volleyball). In the research by Heinecke et al. [15], GT treatment was found to better facilitate the treatment of soft tissue movement limitations, when compared with dynamic stretching and strengthening protocols.

In another study, Laudner et al. [16] argued that limited glenohumeral (GH) range of motion (ROM) occurs during the deceleration phase of overhead throwing due to the repetitive rotational and distractive forces exerted on the posterior shoulder, which can lead to shoulder injuries. IASTM, such as the Graston Technique, was found to be effective for various shoulder injuries and disorders.

In a case study by Terry Loghmani et al. [17], a 55-yr-old male guitarist who had injured the proximal interphalangeal joint of his left index-finger was found to have improved physical measures and function, including an immediate gain in finger range of motion by using GT IASTM alone. This case study demonstrated

Fig. 1 Graston Technique® instrument set (Permission for photo provided by Graston Technique, LLC)

[1]Corresponding author.

Manuscript received November 6, 2016; final manuscript received April 28, 2017; published online July 18, 2017. Assoc. Editor: Rita M. Patterson.

that the manual therapy approaches integrating IASTM could provide an effective conservative treatment strategy for patients with finger-hand conditions in the performing arts and other patient populations.

As a conservative approach, eccentric strengthening exercises have been used for the treatment of Achilles tendinopathy. The recommended treatment period for this approach is typically 12 weeks. Phipps et al. [9], demonstrated the potential effectiveness of IASTM as a manual therapy approach for the treatment of tendon disorders. They showed the potential to yield positive outcomes in a reduced treatment time. However, the treatment regimen in this study included exercise; thus, the effect of IASTM was not isolated. Despite this limitation, the treatment combination yielded positive outcomes in relatively fewer visits. Looney et al. [5] also carried out a research demonstrating that patients with plantar fasciitis treated with GT IASTM and a home stretching program experienced clinically meaningful improvements.

Arthrofibrosis of the knee is a frequent postsurgical complication of total joint replacements that can limit range of motion, inhibit muscle activity, and decrease patient function. In studies by Black [18], GT was used during the rehabilitation to address such arthrofibrotic limitations. Clear improvement in knee range of motion and quadriceps activity and function was found with IASTM intervention.

These studies have shown that the force applied by a clinician is a critical parameter in IASTM treatment and should thus be quantified and measured accurately for research purposes as well as clinical applications. Several human and animal studies have attempted to measure the pressure delivered during soft tissue manipulation using different strategies. An earlier human study by Lee et al. [19] investigated the effect of transverse friction massage (TFM) on flexeor carpi radialis (FCR) motoneuron (MN) pool excitability. They built an electronic system to evaluate the massage rate, momentary pressure, and total cumulative pressure. Their system was based on an ultrathin flexible pressure sensor (ConTacts C500) which was fixed on the thumb of the examiner and insulated by a plastic glove. However, this system could potentially provide inaccurate measurements during clinical use for several reasons: (1) sensor slippage causing aberrant motion and force detection, (2) the force sensed at the practitioner's finger not being the same as that applied to patient's skin, and (3) different therapists having different thumb sizes and softness, which might affect the force measurements.

Recently, in an animal study by Wang et al. [20], an automated device was developed that could generate a certain amount of force with a feedback loop. Force could be applied with either compression or transverse profiles. However, the transverse force measurements were not used as a component of the feedback. The device consisted of a base, where small animal (rats and rabbits) were held during the application, and two movement axes to apply force in the horizontal (X) and vertical (Z) directions were used. Two-axis force sensors, which were based on piezo resistance, were mounted at the bottom end of the Z-axis and measured both compression and tensile forces in X and Z directions. Different stainless steel tips, which could be fixed on the two-axis force sensors, were manufactured according to different tissue size. This bulky equipment provided a useful method to quantify the force delivered to an animal subject in a fixed manner; however, this device system is impractical for clinical usage because of its marked constraints. Also, neglecting the transverse forces could result in inaccurate resultant force readings.

Similarly, another animal study by Zeng et al. [21], constructed a vertical automated compression device, which used a pneumatic system to apply a certain amount of force on a rabbit. A linear motion control system was used to control the generated force, and a force sensor (Pasco Inc., Hudson, OH) provided the feedback to the device. However, this device cannot satisfy the maneuverability, repeatability, and feasibility required for clinical practice.

The primary objective of the work described in this paper was to design, build, and test the accuracy of a force measurement device system for IASTM, and to incorporate other important parameters, such as the tool orientation angles, stroke frequency, and a full monitoring system, using a suitable platform for clinical and research use. The design concepts were intended to enable expansion to other shaped treatment tips for dispersive pressure and use on different shaped body parts. In this paper, two proposed designs of a mechatronic IASTM device system for localized application of pressure, similar to the treatment tip of GT3, as shown in Fig. 2, are presented. The first design used four 1D compression load cells to measure the three force components in the 3D space. The second design used a 3D load cell. The ergonomic casing of the device was designed with CAD tool and 3D printed.

Proposed IASTM Tool Designs

Design Requirements. Several parameters should be considered in the design of the mechatronic IASTM device. The new device should be able to measure forces within 0–155 N in each of the 3D axes, orientation angles (yaw, pitch and roll), treatment time up to 20 min, and stroke frequency during a session within 1–2 Hz. It should be ergonomic, compact, lightweight, and portable. Both length and diameter of the device should not exceed 170 mm and 24 mm, respectively. In addition, the weight should be less than 0.75 kg to make easer for hand movements. From the safety perspective, the new device should run at relatively low voltage up to 5 V to reduce the risk of electric shock on wet skin. The devices must be durable and reusable because of their frequent usage in clinics and affordable at reasonable prices. Finally, the device should have a user interface for reading the parameter measurement in real-time, which is very useful for researchers, students, and therapist. These design requirements need to be considered in all design stages, from component selection to the manufacturing process.

Electronic Component Selection. After considering all design requirements, an extensive research was conducted to reach the optimal designs that could meet the requirements stated in Design Requirements section. The IMUduino (San Francisco, CA) microcontroller board was selected since it can provide the orientation angles and stroke frequency using its Gyro, three-axis digital compass, and accelerometer sensors. As shown in Fig. 3, the IMUduino board had a small form factor (39.8 mm × 15.72 mm) which helped in reducing the device size.

An extensive and wide-ranging search on force sensors was performed to select the appropriate force sensors for the new IASTM tool devices. As a result, the smallest compression load cell and a 3D load cell were considered for force measurements.

The first selected force sensor was a compression load cell (FC-08 as shown in Fig. 4) [23], which was produced by Forsentek Co., Limited, Shenzhen, China. It can measure up to 20 kg of force acting vertically on its nob with a diameter and height of 8 mm and 5 mm, respectively. The output of the load cell was amplified and filtered using a signal conditioning unit.

The second load cell was a 3D load cell (USL06-H5-500 N-C, as shown in Fig. 5(*a*)), which was made by Tec Gihan Co., Ltd., Kyoto, Japan. This load cell could measure forces in three-dimensional space (3D), with force ranges of up to ∓500, ∓500, and +1000 N for X, Y, and Z axis, respectively. An external amplifier (DSA-03 A, as shown in Fig. 5(*b*)) supplied by the same company was used for signal conditioning.

Fig. 2 GT-3 treatment tip (Permission for photo provided by Graston Technique, LLC)

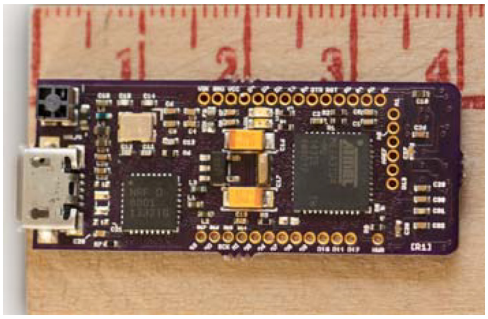

Fig. 3 IMUduino microcontroller

Fig. 4 Small compression load cell (FC-08)

(*a*) (*b*)

Fig. 5 (*a*) The 3D load cell and (*b*) the external amplifier for the 3D load cell

One-Dimensional Compression Load Cell Based Design. After all electronics and sensors were selected, the new designs of the IASTM tool were created using CREO PARAMETRIC 2.0 CAD software. As shown in Fig. 6(*a*), the first model was constructed based on the small compression load cell (FC-08). The load cell placement in the device housing is shown in Fig. 6(*c*). This device consisted of four parts: tip, frame, back cover, and keyways. As shown in Fig. 6(*b*), the tip was designed to be similar to the GT-3 tip, so it had the same precision for targeting soft tissues. A measurement cavity was designed to fit four compression load cells, see Fig. 6(*b*) (only left load cell inserted for demonstration). A back cavity was designed to fit all electronic component sizes needed for the device. A back cover was used to seal and insulate the electronics inside the cavity. The cross section of the frame was narrowed for finger placements in consideration of the overall diameter and sensor placements.

In terms of force measurements, this design used combinations of the compression load cells to measure the three resultant force components in sensors three-dimensional space. The orientation angles of the IASTM device, which had an effect on the force measurements, were considered. Figure 7 presents the orientation angles of the IASTM device with respect to its global coordinates. The angle between the tool and skin generally varied between 20 deg and 70 deg with respect to the *X*–*Y* plane in a typical treatment. The device rotation about the *Z*-axis was considered to be free. The force sensors arrangement was based on the force analysis of the measured forces (see Fig. 7).

According to the orientation constraints, there are three expected movements, each of which produces three different measurements of force. As shown in Fig. 7, various load cells were positioned around the measurement cavity based on force factorization. First, $**S_z+$ and Sy+ load cells measured force components when the force was applied in *Y*–*Z* plane at the tip of the IASTM device, see Fig. 8(*a*). Second, when the force was applied with an angle between 0 deg and 89 deg, three force components were measured by the S_{z+}, S_{x-}, and S_{y+} load cells, as shown in Fig. 8(*b*). Third, when the force was applied with an angle between 91 deg and 180 deg, three force components were measured by the S_{z+}, S_{x+}, and S_{y+} load cells, see Fig. 8(*c*). As a result, this force analysis confirmed that there was no need for the fifth load cell since there was no force component in the directions

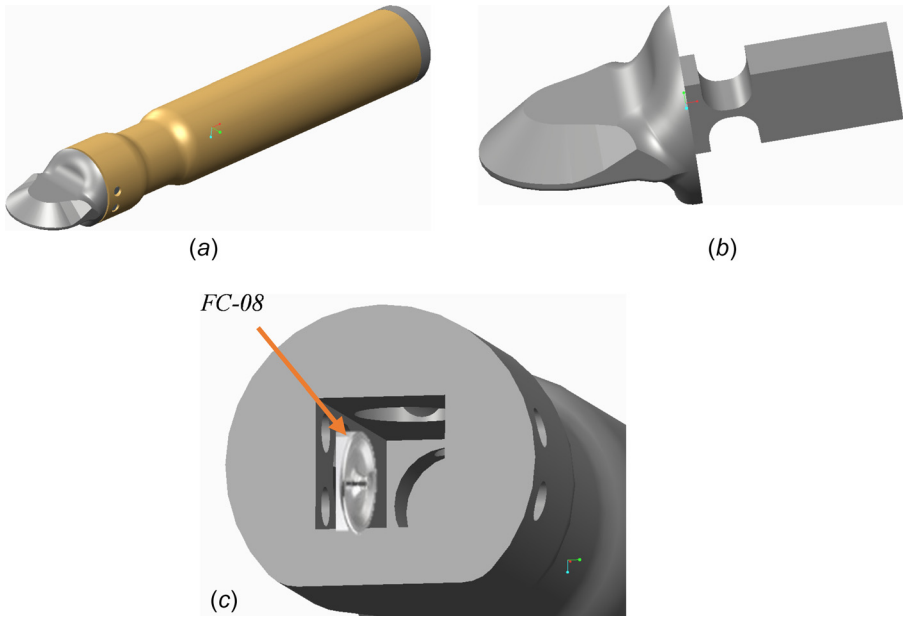

(*a*) (*b*) (*c*)

Fig. 6 (*a*) Device based on the compression load cell, (*b*) tip design for the device based on the compression load cell, and (*c*) sensor placements for the compression load cell mode (only left sensor inserted)

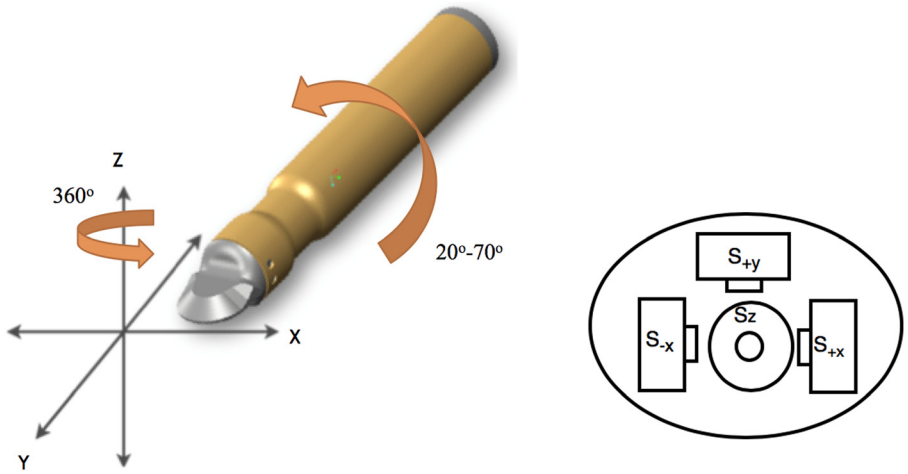

Fig. 7 Mechatronic IASTM device orientation angles and force sensors placement

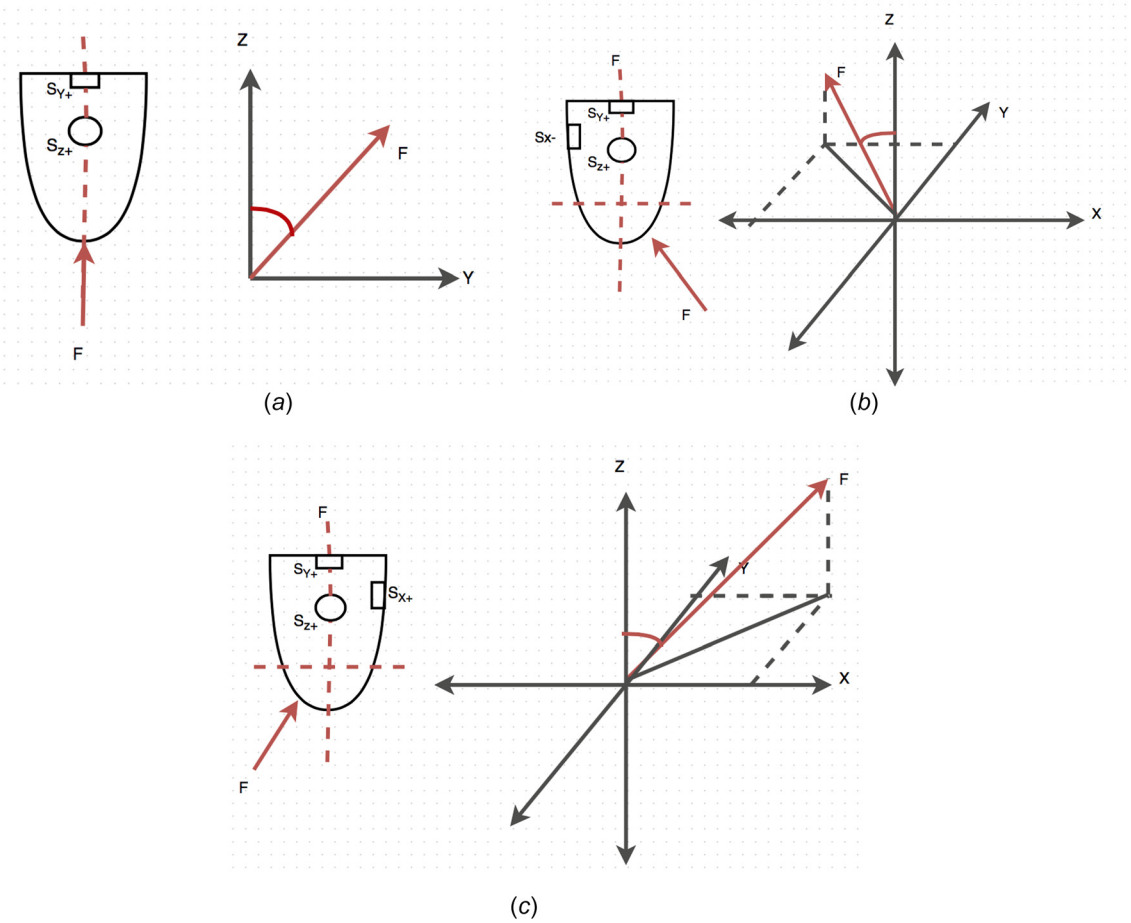

Fig. 8 (*a*) Force analysis for 90 deg force applied to the tool (top left), (*b*) force analysis for 0–89 deg force applied to the tool (top right), and (*c*) force analysis for 91–180 deg force applied to the tool (bottom)

of $-Z$ and $-Y$. This would lead to reduced cost of the 1D compression load cell-based device.

As shown in Fig. 9, the measurement mechanism of the compression load cell device was based on forces measured by a well-placed four compression load cells and a subsequent transformation to an appropriate coordinate system. Three tiny wiring canals were used to connect the wires from the load cell compartment to the microcontroller in the electronics cavity. This design included

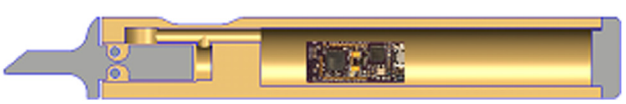

Fig. 9 Full section for the compression load cell device

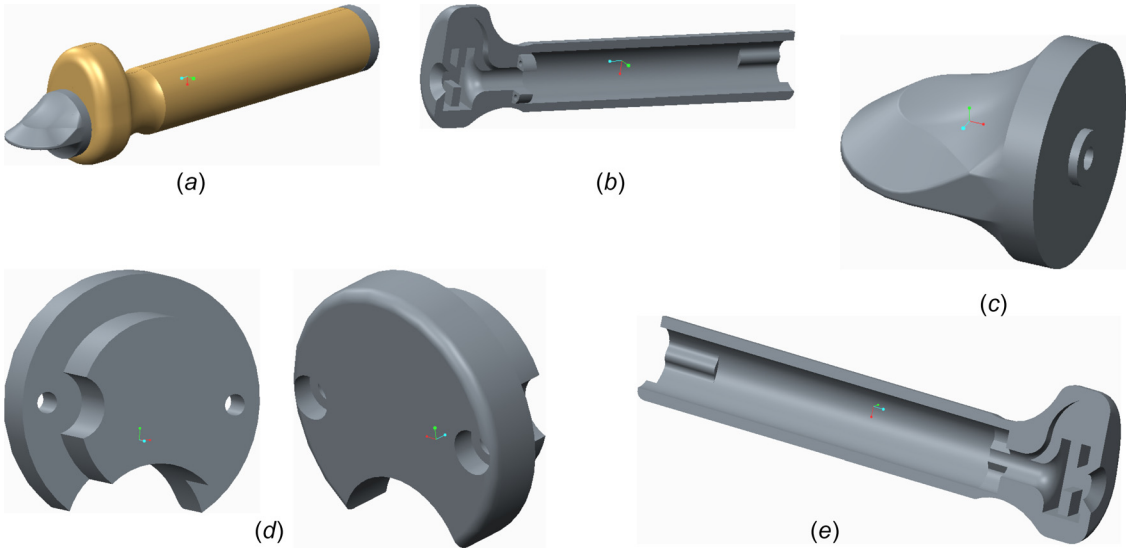

Fig. 10 (*a*) Three-dimensional load cell device (top left), (*b*) three-dimensional load cell device frame parts (top center), (*c*) three-dimensional load cell device tip (top right), (*d*) three-dimensional load cell device back cover (bottom left), and (*e*) three-dimensional load cell device frame parts (bottom center)

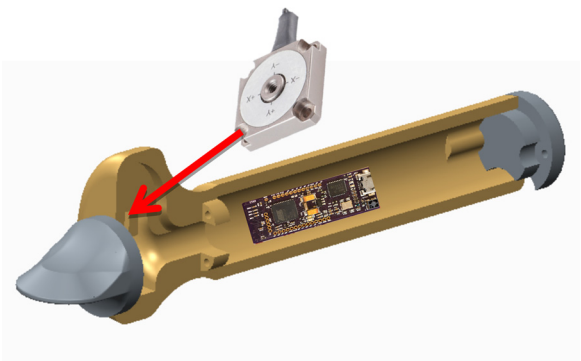

Fig. 11 Half section of the 3D load cell device

two keyway pins to lock the tip to the main frame with 3 mm clearance to allow force transmission.

Three-Dimensional Load Cell-Based Design. The second design was based on a 3D load cell, which was a single load cell that measures all force components. As shown in Fig. 10, the 3D load cell design consisted of three parts similar to the previous model; however, the main frame was separated into two parts for wiring purposes. These frame parts were assembled using two front internal screws and two back external screws for the back cover, as shown in Fig. 10(*b*).

Similar to the compression load cell device, the tip was designed to be similar to the IASTM device tip; as a result, it had the similar precision in targeting soft tissues. A back cavity was designed to fit all electronics and components needed for the main tasks, as shown in Fig. 10(*c*). The back cover was used to seal and insulate the electronics inside the cavity. It had a small crescent shaped outlet hole for the 3D load cell and microcontroller wires, as shown in Fig. 10(*d*). Part of the cross section of the frame had been narrowed for ergonomic finger placement.

In order to measure the force, the 3D load cell was inserted into slots which were designed on both sides of the frame to fit the dimension of the 3D load cell and its wires, as shown in Fig. 11. The tip was attached to the 3D load cell using a fully threaded stainless steel screw, and the contact area was the center part of the 3D load cell with a diameter of 6 mm. As a result, the 3D load cell measured all force components that were being applied to the device's tip. However, the 3D load cell measured the forces applied to its center, and these forces needed be transferred to the tool tip/skin interface.

As shown in Fig. 12(*a*), the 3D load cell-based device had three different coordinate systems: microprocessor, 3D load cell, and tool tip/skin coordinate. The load cell and microcontroller coordinates were based on their datasheets, while the tool-tip/skin coordinate was assumed to have the following sign convention: device forward (+*Y*), right (+*X*), and upward movement (+*Z*), which was based on the right-hand rule.

It was important to transfer the measured forces to the tool-tip/skin interface, because the forces at the skin were the main

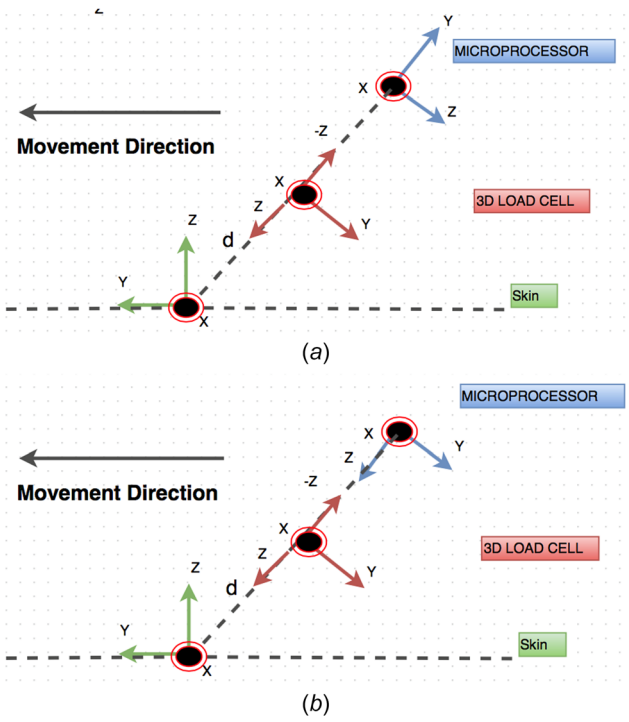

Fig. 12 (*a*) Main coordinates for the 3D load cell device and (*b*) final coordinates for the 3D load cell device

concern for the treatment practice. To perform the force transformation, the microcontroller coordinate was rotated by 90 deg counterclockwise (CCW) about the X-axis to agree with the 3D load cell coordinates, as shown in Fig. 12(*b*). This rotation transformation was performed in IMUduino chip [22]. Next, the orientation angles were used to transfer the force measurement to the tool/skin interface since the microcontroller and the 3D load cell coordinates agreed with each other, as both coordinates were on the same solid body.

Based on the Euler's rotation theorem, any arbitrary rotation (ROT) for a solid object or vector (V) could be represented by a combination of three rotations [24], as shown in the equation given below:

$$V' = \mathrm{ROT}_x \times \mathrm{ROT}_y \times \mathrm{ROT}_z \times V \tag{1}$$

where rotations about the X, Y, and Z axes were computed using Eqs. (2)–(4). The angles yaw, pitch, and roll were represented by y, p, and r letters, respectively. All angles were multiplied by -1, because force components should transfer back to the origin (horizontal plane) of the 3D load cell coordinate after any rotation in the 3D space.

$$\mathrm{ROT}_x = \begin{bmatrix} 1 & 0 & 0 & 0 \\ 0 & \cos d(-p) & -\sin d(-p) & 0 \\ 0 & \sin d(-p) & \cos d(-p) & 0 \\ 0 & 0 & 0 & 1 \end{bmatrix} \tag{2}$$

$$\mathrm{ROT}_y = \begin{bmatrix} \cos d(-r) & 0 & \sin d(-r) & 0 \\ 0 & 1 & 0 & 0 \\ -\sin d(-r) & 0 & \cos d(-r) & 0 \\ 0 & 0 & 0 & 1 \end{bmatrix} \tag{3}$$

$$\mathrm{ROT}_z = \begin{bmatrix} \cos d(-y) & -\sin d(-y) & 0 & 0 \\ \sin d(-y) & \cos d(-y) & 0 & 0 \\ 0 & 0 & 1 & 0 \\ 0 & 0 & 0 & 1 \end{bmatrix} \tag{4}$$

Next, the measurements were transferred to the skin coordinate system with a distance d, which was the distance between the measuring point on the 3D load cell and the tip. Force measurements translation along Z-axis was achieved by using the equation given below:

$$T = \begin{bmatrix} 1 & 0 & 0 & 0 \\ 0 & 1 & 0 & 0 \\ 0 & 0 & 1 & d \\ 0 & 0 & 0 & 1 \end{bmatrix} \tag{5}$$

Then, a CCW rotation about the X-axis was necessary to transfer the force measurements to the proposed practice direction, as shown in the following equation:

$$\mathrm{ROT}_{x_{\mathrm{skin}}} = \begin{bmatrix} 1 & 0 & 0 & 0 \\ 0 & \cos d(90) & -\sin d(90) & 0 \\ 0 & \sin d(90) & \cos d(90) & 0 \\ 0 & 0 & 0 & 1 \end{bmatrix} \tag{6}$$

Finally, to get the transformed force measurement on the skin surface, the force vector was multiplied by the distance matrix, the Euler's rotation matrix, and the assumed practice direction matrix, respectively, as shown in Eq. (7). Equation (6) was used to transfer the force measurement (F) to the skin coordinate (F')

$$F' = \mathrm{ROT}_{x_{\mathrm{skin}}} \times \mathrm{ROT}_x \times \mathrm{ROT}_y \times \mathrm{ROT}_z \times T \times F \tag{7}$$

Equation (7) was computed using MATLAB, to represent each force component in a separate formula, as shown in the following equations:

$$F'_x = d \times \sin d(-r) + F_z \times \sin d(-r) + F_x \times \cos d(-r) \times \cos d(-y) - F_y \cos d(-r) \times \sin d(-y) \tag{8}$$

$$F'_y = -F_x \times (\sin d(-p) \times \sin d(-y) - \cos d(-p) \times \cos d(-y) \times \sin d(-r)) - F_y \times (\cos d(-y) \times \sin d(-p) + \cos d(-p) \times \sin d(-r) \times \sin d(-y)) - F_z \times \cos d(-p) \times \cos d(-r) - d \times \cos d(-p) \times \cos d(-r) \tag{9}$$

$$F'_z = F_x \times (\cos d(-p) \times \sin d(-y) + \cos d(-y) \times \sin d(-p) \times \sin d(-r)) + F_y \times (\cos d(-p) \times \cos d(-y) - \sin d(-p) \times \sin d(-r) \times \sin d(-y)) - F_z \times \cos d(-r) \times \sin d(-p) - d \times \cos d(-r) \times \sin d(-p) \tag{10}$$

To verify and examine these formulas, different orientation angles were proposed under measured 100 N compression force and substituted in the overall force transformation matrix, as shown in Table 1. The calculated data from Eq. (10) were broadly consistent with conceptually expected values.

An external amplifier (DSA-03A) was used to filter and amplify the output signals of the 3D load cell, which were then introduced to the LABVIEW software using the data acquisition card (DAQ), as shown in Fig. 13. In addition, the microcontroller (IMUduino), that measures the orientation angles, was connected directly to the computer (PC) using a USB cable.

The 3D load cell sensor measured strains in the 3D space. The force components were obtained by multiplying strain readings in 3D space by the sensor specific calibration matrix, as shown in Eq. (11). However, the sensor output was in volts, where 1 V was equal to 400 microstrains.

$$\begin{bmatrix} F_x \\ F_y \\ F_z \end{bmatrix} = \begin{bmatrix} 0.23017 & -0.00226 & 0.00360 \\ 0.01763 & 0.22724 & -0.00208 \\ -0.00267 & 0.00122 & 0.26504 \end{bmatrix} \begin{bmatrix} \varepsilon_x \\ \varepsilon_y \\ \varepsilon_z \end{bmatrix} \tag{11}$$

F_x, F_y, F_z: load value (Newton) on the 3D load cell's tip; ε_x, ε_y, ε_z: strain output ($\times 10^{-8}$ strain).

Table 1 Resultant forces expected on skin with different orientation angles under 100 N compression force

Only rotation	Force (N)	Combination (rotation and translation)	Force (N)
Yaw = 0	$F_x = 0$	Yaw = 0	0
Pitch = 0	$F_y = 100$	Pitch = 45	69.2965
Roll = 0	$F_z = 0$	Roll = 0	−69.2965
		Trans-z = 2	
Yaw = 0	$F_x = 0$	Yaw = 0	0
Pitch = 45	$F_y = 70.71$	Pitch = 45	67.8823
Roll = 0	$F_z = -70.71$	Roll = 0	−67.8823
		Trans-z = 4	
Yaw = 0	$F_x = 70.71$	Yaw = 0	0
Pitch = 0	$F_y = 70.71$	Pitch = 45	66.4680
Roll = 45	$F_z = 0$	Roll = 0	−66.4680
		Trans-z = 6	
Yaw = 45	$F_x = 0$	Yaw = 0	66.4680
Pitch = 0	$F_y = 100$	Pitch = 0	66.4680
Roll = 0	$F_z = 0$	Roll = 45	0
		Trans-z = 6	

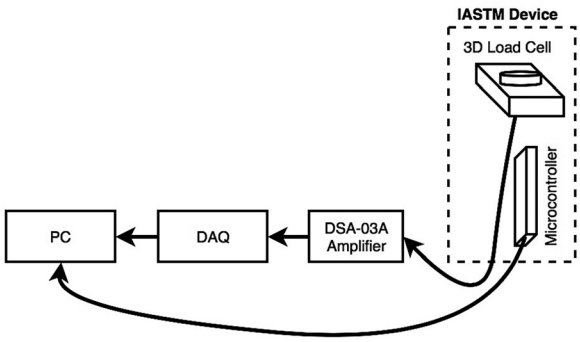

Fig. 13 Three-dimensional load cell device system configuration

Design Selection. After both designs have been investigated and all components selected based on the design requirements, the 3D load cell-based device has been selected for prototyping for several reasons. The electronics integration of the 1D compression load cell-based design needed more signal conditioning. This would increase the space inside the device resulting in the larger device profile. On the other hand, the 3D load cell-based device came with its own external signal conditioning unit, provided by the sensor manufacturer. Additionally, the 3D load cell-based design provided measurements with greater degree of accuracy. The 1D compression load cell-based design will be revisited in the future studies to make it functionally and economically competitive with the 3D load cell-based design.

LABVIEW Model Building for 3D Load Cell Device

Force Measurement Model. The force measurement was filtered and amplified using the external amplifier (DSA-03A), which provided the force variation in terms of voltage within ∓ 5 V for the three axes using three cables. These cables were connected to the DAQ device, and a LABVIEW model was created to get the final force measurement for each axis. The force measurement model consisted of three phases: signal enquiring, gains multiplication and calibration and transformation. DAQ ASSISTANT software on the PC was used in a while loop to extract continuously the force signal from the DAQ and send it to the LABVIEW model. The DAQ ASSISTANT displayed the input signals, which were adjusted to zero using the external amplifier's trimmers. Then, two different gains were multiplied by the input signals. The gains for the X- and Y-axes were 200 each, and 400 was the gain for the Z axis according to the manufacturer. Then, force signals were stored in a matrix form and multiplied by the calibration matrix (11). The resultant force was translated along the Z-axis and rotated around the X-axis 90 deg using the Euler's rotation matrix with a rotation order of X–Y–Z, respectively.

Orientation Measurement Model. The IASTM orientation angles were measured using the IMUduino microcontroller, which used the open source modified code Free IMU-Yaw-Pitch-Roll. The Arduino code sent the measured angles to LABVIEW using a serial USB cable in a specific modified form (xYAWyROLLz-PITCH). In LABVIEW, a model was developed to interpret the previous angle measurement string, which was sent to LABVIEW by the IMUduino. The orientation measurement model extracted the angles based on the placements of the three characters x, y, and z.

The IASTM Measurement Model. The force and orientation measurement models were assembled in one final model in LABVIEW, to obtain the instantaneous angles for the force transformation. In this paper, only pitch angle was considered in the force transformation, because it was the critical parameter in the IASTM practice; roll and yaw angles were assumed to be zero. Besides angle and force measurements, the mechatronic IASTM device provided additional data, which included critical parameters in the treatment. These parameters include average angles, average forces of last 200 samples, maximum and minimum measured force for each axis, resultant force using Eq. (12), average peak resultant force, stroke number, and stroke frequency per minute.

$$\text{Resultant force} = \sqrt{F_x^2 + F_y^2 + F_z^2} \tag{12}$$

The stroke counter used the peak detection for the measured force of Z-axis function in LABVIEW, where the threshold and signal width were set to be 5 N and 3 s, respectively. All measurements could be exported in Excel format file for practice analysis. As shown in Fig. 14, a user-friendly front panel was created to present all necessary data for the clinician during IASTM practice.

IASTM Casing Fabrication Using 3D Printing Technology. The prototypes of the proposed designs were fabricated using 3D printing technology (see Figs. 15(*a*) and 15(*b*)). Three-dimensional printing was performed using the CAD design to print layer by layer until the models were completed, using fused deposition modeling (FDM). All hung parts and cavities were filled by the printer with removable supporting materials that were removed using hand tools and specific solutions. All CAD files were transformed into stereolithography (STL) format using CREO PARAMETRIC 2.0. A 3D printer (uPrint SE) and ABS material were used to fabricate both designs after uploading STL files to CATALYSTEX software. Both the printer and software were made by Stratasys.

Measurements Validation Test

The 3D compression load cell-based IASTM was selected to be assembled and tested for accuracy and repeatability. The applied force and angle are quantified. Accurate force and angle measurement would allow the new IASTM device to standardize the

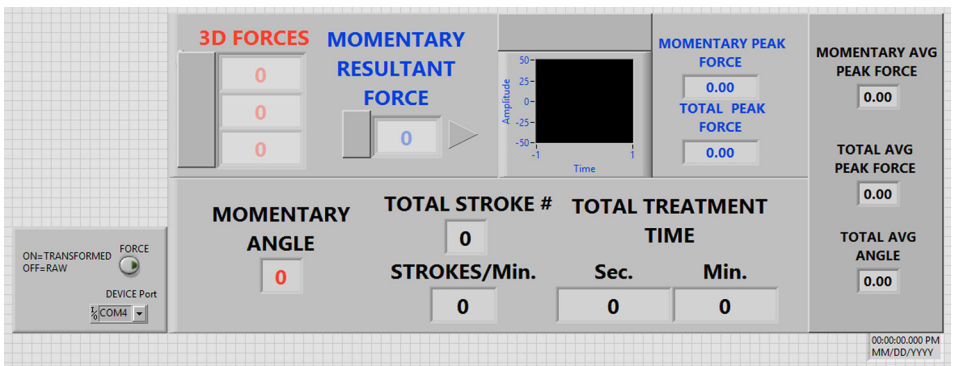

Fig. 14 The IASTM device front panel

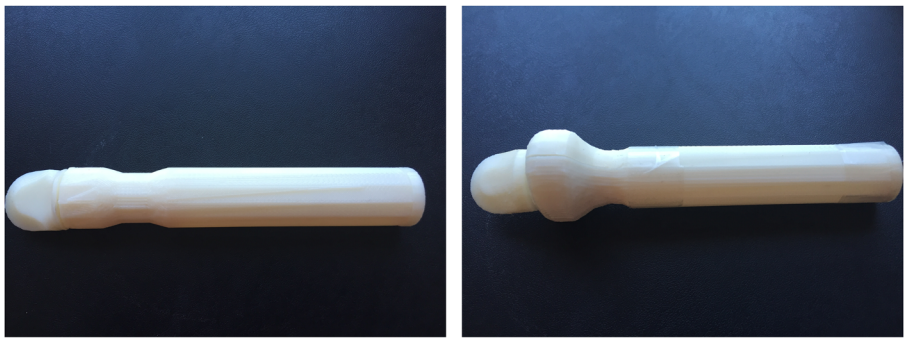

(*a*) (*b*)

Fig. 15 (*a*) Three-dimensional printed model of compression load cell device and (*b*) three-dimensional printed model of 3D load cell device

(*a*) (*b*)

Fig. 16 (*a*) Electronic scale and (*b*) combination square set (angle validation system)

Table 2 Summary of the scale accuracy test

The scale accuracy			
	Scale measured		
Weight (g)	Gram (g)	Newton (N)	Relative error %
150.00	150.00	1.50	0.00
200.00	200.00	2.00	0.00
250.00	250.00	2.50	0.00
300.00	300.00	3.00	0.00
350.00	350.00	3.50	0.00
400.00	400.00	4.00	0.00
1019.72 (10 N)	1000.00	10.00	−1.93
1369.72 (10 N + 350)	1350.00	13.00	−1.44
1419.72 (10 N + 400)	1400.00	13.50	−1.39
1469.72 (10 N + 450)	1500.00	14.50	2.06

Table 3 Scale data format

Digit	1	2	3	4	5	6	7	8	9	10	11	12	13	14	15	16
Data	∓	Space	Measured value								Space	—	Unit		CR	LF

IASTM practice and move it to the next level, which is a human study.

Force Validation System. A force validation system was built to ensure that the IASTM device could meet the force measurement requirements. The force component on *Z* direction (perpendicular to skin surface) was selected to be validated. The system was based on electronic scale (PCE-PB 150 N) with readability of 0.49 N to measure the vertical force component on the scale plate, as shown in Fig. 16(*a*). Different weights were placed on the scale to check the scale accuracy. As shown in Table 2, the scale could not detect any load less than 100 g. However, the relative error varied between 0% and 2.06% for the rest of the load measurements.

The scale measurement in Newton was acquired using LABVIEW software through a serial port interface. According to the scale manufacturer, the communication protocol is shown in Table 3. The 8-bit force measurement was placed between the third and tenth byte. The measurement unit was stored in bit 13 and 14. As a result, a LABVIEW model was constructed to extract the scale measurement based on this protocol. The force applied is also measured by the IASTM device and transmitted to the LABVIEW model. The readings from the scale and the IASTM are compared and displayed on LABVIEW user interface.

Orientation Angle Validation System. A validation system was built to ensure that the IASTM device met the angle measurement requirements. As shown in Fig. 16(*b*), the combination square set was set on flat surface.

Methodology and Test Results

Three student examiners from the Indiana University School of Health and Rehabilitation Science Physical Therapy Department at IUPUI used the new IASTM device system to apply force to the scale plate at different pitch angles. In the first and second tests, each student was asked to apply as much force as possible

five times through the IASTM device with a pitch angle between 85 deg and 95 deg (holding the device perpendicular to the scale surface) using a pencil grip hand position, as shown in Fig. 17. The 3D load cell and scale measurements were recorded. Accuracy of the measurement was investigated by observing the absolute relative error, which varied between 0% and 5.9%. To evaluate the measurement repeatability, each student was asked to target specific force application on the scale multiple times for four trials. The force measurements for the first two experiments are shown in Figs. 18 and 19, respectively. The vertical black bar is the range of the force read from IASTM multiple times in the same trial. The yellow dots in the figure represent the digital scale readout. The close proximity of the tool-measured forces and the digital scare reading indicate that the tool offered acceptable degree of repeatability.

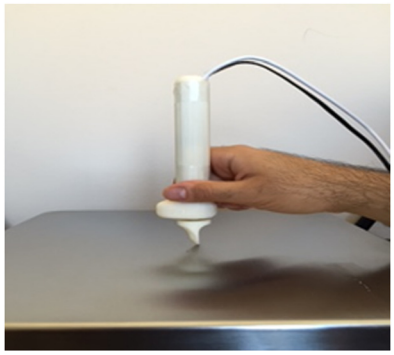

Fig. 17 Hand position of IASTM device in the first and second tests configuration

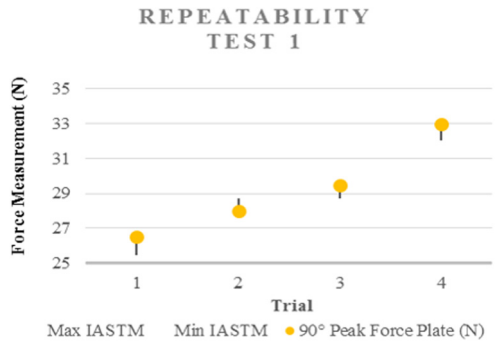

Fig. 18 First repeatability test (see color figure online)

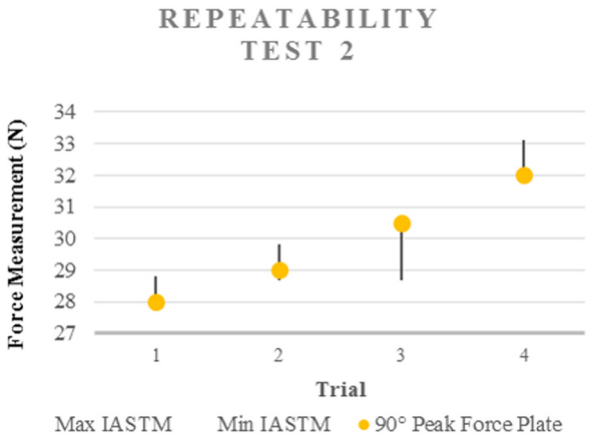

Fig. 19 Second repeatability test (see color figure online)

In the third test, each examiner was asked to apply as much force as possible but the IASTM device's pitch angle had to be within 40–50 deg using a pencil grip hand position, as shown in Fig. 20. An exercise mat was inserted between the scale plate and device's tip to simulate the skin response. The 3D load cell and scale measurement were exported. The absolute relative error varied between 2.74% and 11.43%. The students were asked to target specific measurements on the scale multiple times for three trials to evaluate the repeatability. The force measurement was quite repeatable, as shown in Fig. 21. Both the maximum absolute relative error and measurements repeatability were affected by the existence of the exercise mat. The maximum absolute relative error was higher than the previous test, and the force measurement varied along a baggier range of measurement in one of the trials. These test results indicated the IASTM device had high repeatability and accuracy.

For angle measurement, the IASTM device was attached to a ruler arm of the combination square set at three different angles, 30 deg, 45 deg, and 60 deg, as shown in Fig. 22. The indicated pitch angle from the combination square set and the measured pitch angle from the LABVIEW were compared, as shown in Table 4. The absolute relative error varied between 1.6% and 3.3%. The angle test results indicated that the IASTM device had an accurate pitch angle measurement.

After force and angle measurements were proven to be effective and accurate, the dynamic analysis was performed using the IASTM device. An examiner was asked to apply a random number of force strokes to skin with an approximated pitch angle of 45 deg. As shown in Fig. 23, the F_z and F_y force components on the skin surface (skin coordinate) were almost identical during the test time, which was 21.5 s, because the pitch angle was approximately 45 deg and that would distribute the applied force equally

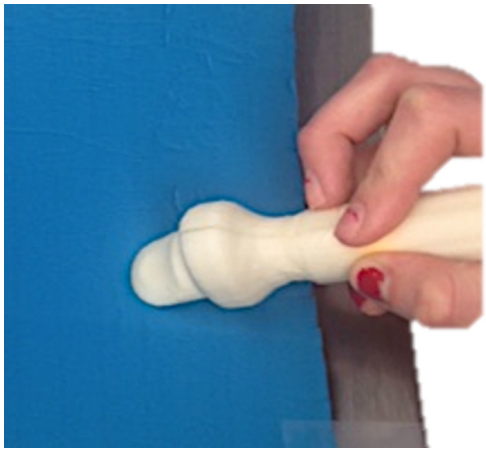

Fig. 20 Hand position of IASTM device in the third test

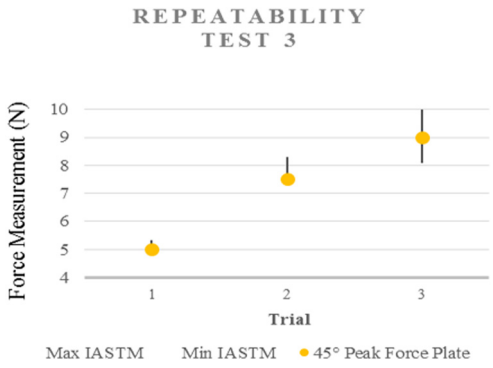

Fig. 21 Third repeatability test

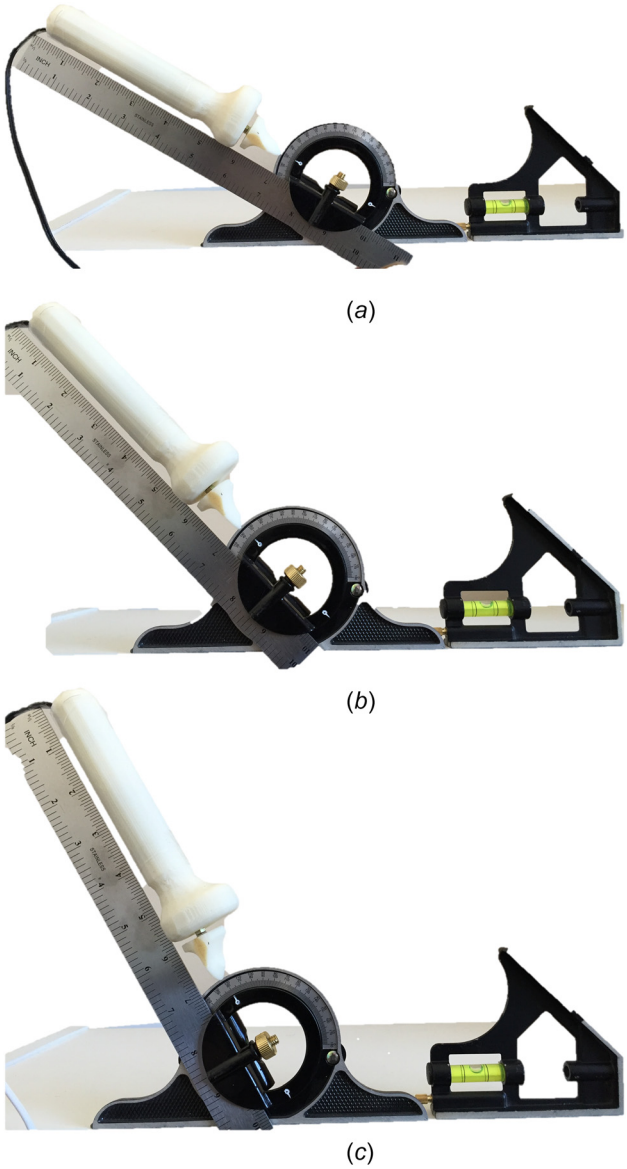

(*a*)

(*b*)

(*c*)

Fig. 22 IASTM device at 30 deg (top), 45 deg (middle), and 60 deg (bottom)

Table 4 Summary pitch angle measurement test

Indicated pitch angle (deg)	Measured pitch angle (deg)	Relative error (%)
30	29	−3.33
45	46	2.22
60	61	1.6

for the F_z and F_y components. The examiner attempted to maintain the device at 45 deg during the test; however, every time the IASTM device interacted with the skin, the examiner's hand tilted the device to approximately 50 deg. The test has proven that the 3D compression load cell-based IASTM device has succeeded in measuring both force components and device's orientation angle simultaneously. In addition, the implemented force transformation equations (8)–(10) have successfully transformed the force measurements from 3D load cell's tip coordinates to the skin coordinates. The new device was able to track the measured force and display in the visual interface.

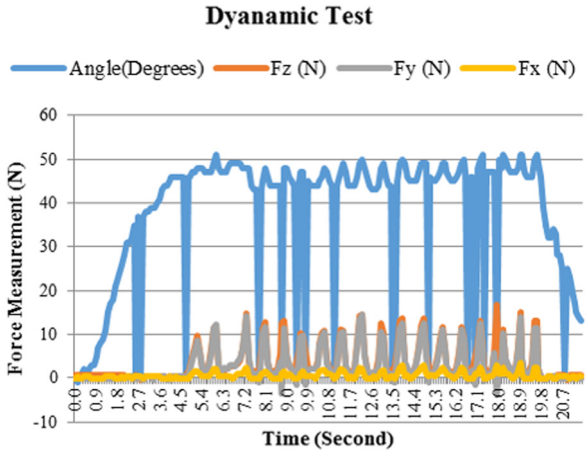

Fig. 23 Summary of the dynamic test for the IASTM device

Conclusion

IASTM is a type of massage, i.e., a form of mechanotherapy, which uses rigid manufactured or cast devices to deliver force to the tissue. Hence, the treatment force is a critical parameter during massage applications, but has not been objectively measured or standardized in a clinically relevant manner. In addition to force magnitude, the angle of force application and stroke frequency play an important role during IASTM. There is a strong need to characterize the forces delivered to a patient, including the angle of treatment and stroke frequency. This paper presented two novel designs of IASTM devices that can quantify localized pressure to the soft tissue. The first design used four compression load cells to measure the three force components in three-dimensional space. The second design used a 3D load cell to measure all three component forces. Force and orientation measurements were transferred to a portable laptop using a data acquisition card from National Instruments. The 3D load cell-based design was selected for implementation which used an IMUduino microcontroller board to measure IASTM orientation angles and to compute stroke frequency. The force and orientation measured in IASTM coordinate systems were transformed and represented with respect to the skin coordinate system. LABVIEW software was used to program and display all required measurements in a user-friendly interface. An electronic plate scale was used to measure known applied forces for device validation which was limited to validating the force component in Z direction (perpendicular to surface) during static testing against an inanimate, external reference. The load cell measurements and the scale reading were compared to determine the accuracy of the IASTM device. The relative error varied between 0% and 11%. The angle measurement was tested using a combination square set tool, and the relative error varied between 0% and 3.3%. The mechatronic IASTM device was found to be accurate, repeatable, and stable during real-time, dynamic operation mode.

References

[1] Davidson, C. J., Ganion, L. R., Gehlsen, G. M., Verhoestra, B., Roepke, J. E., and Sevier, T. L., 1997, "Rat Tendon Morphologic and Functional Changes Resulting From Soft Tissue Mobilization," Med. Sci. Sports Exercise, **29**(3), pp. 313–319.

[2] Gehlsen, G. M., Ganion, L. R., and Helfst, R., 1999, "Fibroblast Responses to Variation in Soft Tissue Mobilization Pressure," Med. Sci. Sports Exercise, **31**(4), pp. 531–535.

[3] Loghmani, M. T., and Warden, S. J., 2009, "Instrument-Assisted Cross Fiber Massage Accelerates Knee Ligament Healing," J. Orthop. Sports Phys. Ther., **39**(7), pp. 506–514.

[4] Loghmani, M. T., and Warden, S. J., 2013, "Instrument-Assisted Cross Fiber Massage Increases Tissue Perfusion and Alters Microvascular Morphology in the Vicinity of Healing Knee Ligaments," BMC Complementary Altern. Med., **13**(1), p. 240.

[5] Looney, B., Srokose, T., Fernandez-De-Las-Peas, C., and Cleland, J. A., 2011, "Graston Instrument Soft Tissue Mobilization and Home Stretching for the Management of Plantar Heel Pain: A Case Series," J. Manipulative Physiol. Ther., **34**(2), pp. 138–142.
[6] Bayliss, A. J., Klene, F. J., Gundeck, E. L., and Loghmani, M. T., 2011, "Treatment of a Patient With Post-Natal Chronic Calf Pain Utilizing Instrument-Assisted Soft Tissue Mobilization: A Case Study," J. Man. Manipulative Ther., **19**(3), pp. 127–134.
[7] McCrea, E. C., and George, S. Z., 2010, "Outcomes Following Augmented Soft Tissue Mobilization for Patients With Knee Pain: A Case Series," Orthop. Phys. Ther. Pract., **22**(2), pp. 69–74.
[8] Burke, J., Buchberger, D. J., Carey-Loghmani, M. T., Dougherty, P. E., Greco, D. S., and Dishman, J. D., 2007, "A Pilot Study Comparing Two Manual Therapy Interventions for Carpal Tunnel Syndrome," J. Manipulative Physiol. Ther., **30**(1), pp. 50–61.
[9] Phipps, R. L., Carney, S. R., Loghmani, M. T., and Bayliss, A. J., 2011, "An Innovative Manual Therapy Approach for the Treatment of Patients With Achilles Tendinopathy: A Case Series," J. Orthop. Sports Phys. Ther., **41**(1), pp. A65–A66.
[10] Kumar, S., Beaton, K., and Hughes, T., 2013, "The Effectiveness of Massage Therapy for the Treatment of Nonspecific Low Back Pain: A Systematic Review of Systematic Reviews," Int. J. Gen. Med., **6**, p. 733.
[11] Crane, J. D., Ogborn, D. I., Cupido, C., Melov, S., Hubbard, A., Bourgeois, J. M., and Tarnopolsky, M. A., 2012, "Massage Therapy Attenuates Inflammatory Signaling After Exercise-Induced Muscle Damage," Sci. Transl. Med., **4**(119), pp. 13–119.
[12] Best, T. M., Crawford, S. K., Haas, C., Charles, L., and Zhao, Y., 2014, "Transverse Forces in Skeletal Muscle With Massage-Like Loading in a Rabbit Model," BMC Complementary Altern. Med., **14**, pp. 1–9.
[13] Graston Technique, 2016, "Graston Technique Advantages," Graston Technique, Indianapolis, IN, accessed Feb. 21, 2017, http://www.grastontechnique.com/home
[14] Graston Technique, 2016, "History of Graston Technique," Graston Technique, Indianapolis, IN, accessed Feb. 21, 2017, http://www.grastontechnique.com/history
[15] Heinecke, M. L., Thuesen, S. T., and Stow, R. C., 2014, "Graston Technique on Shoulder Motion in Overhead Athletes," J. Undergrad. Kinesiology Res., **1**(10), pp. 27–39.
[16] Laudner, K., Compton, B. D., McLoda, T. A., and Walters, C. M., 2014, "Acute Effects of Instrument Assisted Soft Tissue Mobilization for Improving Posterior Shoulder Range of Motion in Collegiate Baseball Players," Int. J. Sports Phys. Ther., **9**(1), pp. 1–7.
[17] Terry Loghmani, M., Bayliss, A. J., Clayton, G., and Gundeck, E., 2015, "Successful Treatment of a Guitarist With a Finger Joint Injury Using Instrument-Assisted Soft Tissue Mobilization: A Case Report," J. Man. Manipulative Ther., **23**(5), pp. 246–253.
[18] Black, D. W., 2010, "Treatment of Knee Arthrofibrosis and Quadriceps Insufficiency After Patellar Tendon Repair: A Case Report Including Use of the Graston Technique," Int. J. Ther. Massage Bodywork: Res. Educ. Pract., **3**(2), pp. 14–21.
[19] Lee, H. M., Wu, S. K., and You, J. Y., 2009, "Quantitative Application of Transverse Friction Massage and Its Neurological Effects on Flexor Carpi Radialis," Man. Ther., **14**(5), pp. 501–507.
[20] Wang, Q., Zeng, H., Best, T. M., Haas, C., Heffner, N. T., Agarwal, S., and Zhao, Y., 2014, "A Mechatronic System for Quantitative Application and Assessment of Massage-Like Actions in Small Animals," Ann. Biomed. Eng., **42**(1), pp. 36–49.
[21] Zeng, H., Butterfield, T. A., Agarwal, S., Haq, F., Best, T. M., and Zhao, Y., 2008, "An Engineering Approach for Quantitative Analysis of the Lengthwise Strokes in Massage Therapies," ASME J. Med. Devices, **2**(4), p. 041003.
[22] Femto, 2016, "IMUduino," Femto, San Francisco, CA, accessed Feb. 21, 2016, http://femto.io/products
[23] Forsentek, 2016, "Micro Compression Load Cell Force Sensor 5 kg 10 kg 20 kg 50 kg 100 kg," Forsentek Co., Shenzhen, China, accessed Feb. 21, 2016, http://www.forsensor.com/
[24] Spong, M., Hutchinson, S., and Vidyasagar, M., 2006, *Robot Modeling and Control*, Wiley, Hoboken, NJ.